

The Proton Gluon Distribution from the Color Dipole Picture

G.R. Boroun

*Department of Physics, Razi University,
Kermanshah 67149, Iran*

M. Kuroda

*Center for Liberal Arts, Meiji Gakuin University
Yokohama, Japan*

Dieter Schildknecht

*Fakultät für Physik, Universität Bielefeld
D-33501 Bielefeld, Germany*
and

*Max-Planck-Institut für Physik (Werner-Heisenberg-Institut)
Föhringer Ring 6, D-80805 München, Germany*

(Dated: August 2, 2022)

Employing the representation of the experimental data on deep inelastic electron-proton scattering (DIS) in the color-dipole picture (CDP), we determine the gluon distribution of the proton at small Bjorken x . At sufficiently large momentum transfer, Q^2 , the extracted gluon distribution fulfills the evolution equation for the proton structure function. For low values of Q^2 , e.g. for $Q^2 = 1.9\text{GeV}^2$, the evolution equation for the proton structure function requires a strong modification of predicted magnitude. The standard procedure of adopting a low- Q^2 input scale for the extraction of the gluon density is highly questionable. Without modification at low Q^2 , the evolution is inconsistent with the required low- Q^2 decrease of the longitudinal structure function with decreasing momentum transfer Q^2 .

I. INTRODUCTION

The extraction of the gluon-distribution function [1–4] of the proton from deep-inelastic electron-proton scattering (DIS) [5] rests on the determination of the fit parameters in an ad-hoc parametrization of the gluon x -distribution at a low- Q^2 input scale.¹ It is well-known, and was recently emphasized [6] that the results on the gluon distribution function from different collaborations [1–4] show a significant spread in the low- x , low- Q^2 domain. The quality of the fits is considered not to be satisfactory. This led to the introduction of phenomenological power corrections [7, 8] to the structure functions, and to modifications [6] of the DGLAP evolution equations [9] for the gluon distribution by a non-linear term [10, 11].

Rather than applying ad hoc modifications to the evolution equations at low Q^2 , it seems appropriate to employ a representation of the proton structure functions at low- x that smoothly connects the regions of large- Q^2 , where perturbative QCD (pQCD) is expected to be valid, and of low- Q^2 .

A representation, unique in this respect, is the color-dipole picture (CDP) [12], [13], [14], [15]. The CDP,

originating from Generalized Vector Dominance (GVD) [16],² smoothly connects the representation of the proton structure functions at high Q^2 , dominantly due to scattering of high-mass fluctuations³ of the (virtual) photon, with the representation at low- Q^2 , including $Q^2 = 0$, where the interaction is essentially due to the scattering of the low-lying vector mesons ρ^0 , ω and ϕ .

In the present paper, accordingly, the leading order gluon distribution is extracted from the representation of the proton structure functions $F_2(x, Q^2)$ and $F_L(x, Q^2)$ in the CDP.

In Section 2, we briefly review the determination of the gluon distribution at leading order of $\alpha_s(Q^2)$ from the pQCD improved parton model. In Section 3, we review the relevant parts of the CDP. In Section 4, we summarize the Froissart-bounded representation of $F_2(x, Q^2)$. In Section 5, the results obtained for the gluon distribution are presented. At low Q^2 ($Q^2 = 1.9\text{GeV}^2$), we observe drastic differences between our results and the results [6] based on the application of ad hoc modifications of the gluon evolution equations. Note that for the results in Sections 2 to 5, no use is being made of the pQCD evolution equations [9].

¹ In standard notation, the virtuality of the photon is denoted by Q^2 , and x is the Bjorken scaling variable, $x \cong Q^2/W^2$, where W denotes the virtual-photon-proton center of mass energy.

² For a more recent review see ref. [17]

³ See ref.[18] for a detailed quantitative estimate of the range of masses of $q\bar{q}$ fluctuation for given $Q^2 \geq 0$.

In Sections 6 and 7, we examine the consistency between the low- Q^2 dependence at low- x of our results for the gluon distribution and the validity of the evolution equation for the structure function $F_2(x, Q^2)$. At large Q^2 , specifically for approximately $20 \text{ GeV}^2 \lesssim Q^2 \lesssim 100 \text{ GeV}^2$, the gluon distribution is consistent with the validity of evolution, leading to the important constraint of $C_2 = 0.29$ for the exponent in the dependence of $F_2(x, Q^2)$ on $(W^2)^{C_2} = (Q^2/x)^{C_2}$, where the predicted value of $C_2 \cong 0.29$ agrees with experiment. At low- Q^2 , the evolution equation for the structure function $F_2(x, Q^2)$ requires an explicitly given modification to decrease the logarithmic derivative of $F_2(x, Q^2)$ by a factor up to about 0.5. Final Conclusions are presented in Section VIII.

II. THE DETERMINATION OF THE GLUON DISTRIBUTION FUNCTION IN PQCD.

In the low- x approximation of the perturbative QCD (pQCD)-improved parton model, the longitudinal structure function of the proton, $F_L(x, Q^2)$, solely depends [14, 19] on the gluon density of the proton,

$$F_L(x, Q^2) = \frac{\alpha_s(Q^2)}{3\pi} \sum_q Q_q^2 I_g(x, Q^2) \quad (2.1)$$

where

$$I_g(x, Q^2) \equiv \int_x^1 \frac{dy}{y} \left(\frac{x}{y} \right)^2 \left(1 - \frac{x}{y} \right) G(y, Q^2), \quad (2.2)$$

the gluon density being denoted by

$$G(x, Q^2) \equiv xg(x, Q^2). \quad (2.3)$$

In standard notation, $\alpha_s(Q^2)$ stands for the strong coupling and the sum $3 \sum_q Q_q^2 \equiv R_{e^+e^-}$ runs over the squared charges Q_q^2 of the actively contributing quarks, $\sum_q Q_q^2 = 10/9$ for four flavors of quarks. See Section 6 for a justification in the case of the CDP of the validity of the approximation of $F_L(x, Q^2)$ in (6.1) by $F_L(x, Q^2)$ given in (2.1).

For a wide range of different gluon distributions, independently of their specific form, the integration in (2.2) yields the well-known approximate result [14, 19] for the longitudinal structure function (2.1)

$$F_L(\xi_L x, Q^2) = \frac{\alpha_s(Q^2)}{3\pi} \sum_q Q_q^2 G(x, Q^2). \quad (2.4)$$

A given gluon distribution determines the longitudinal proton structure function at a rescaled value of $x \rightarrow \xi_L x$. The rescaling factor ξ_L in (2.4) has the preferred value of $\xi_L \cong 0.40$ [19].

Solving (2.4) for $G(x, Q^2)$, allows one to deduce the gluon distribution from measurements of the longitudinal structure function,

$$\begin{aligned} \alpha_s(Q^2)G(x, Q^2) &= \sum_q \frac{3\pi}{Q_q^2} F_L(\xi_L x, Q^2) \\ &= \sum_q \frac{3\pi}{Q_q^2} \frac{R}{1+R} F_2(\xi_L x, Q^2), \end{aligned} \quad (2.5)$$

where in the second step, the longitudinal structure function was replaced by the proton structure function $F_2(\xi_L x, Q^2)$ and the longitudinal-to-transverse ratio,

$$R \equiv \frac{F_L(\xi_L x, Q^2)}{F_T(\xi_L x, Q^2)}. \quad (2.6)$$

A given (analytic) representation of the experimentally measured results for $F_L(x, Q^2)$, or for $F_2(x, Q^2)$ combined with R , according to (2.5), allows one to deduce an (analytic) expression for the gluon-distribution function.

The accuracy of the approximation of (2.1) by (2.4) for a specific gluon distribution derived from (2.5) for a given structure function $F_L(\xi_L x, Q^2)$, may be tested by inserting the result for the gluon distribution deduced from (2.5) into (2.1) (with (2.2)), to subsequently compare the result for $F_L(x, Q^2)$ obtained from (2.1) with the (experimentally confirmed) structure function that originally entered (2.5) in the determination of the gluon distribution. See Section 6 for the explicit representation of this consistency check for the gluon distribution of the CDP.

III. THE COLOR-DIPOLE REPRESENTATION.

We start by a discussion of the results for the photoabsorption cross section, $\sigma_{\gamma^*p}(W^2, Q^2)$, in the CDP that are shown in Fig. 14, reproduced from refs. [14, 15]. The results are obtained from the explicit analytic expression for $\sigma_{\gamma^*p}(W^2, Q^2)$,

$$\begin{aligned} \sigma_{\gamma^*p}(W^2, Q^2) &= \sigma_{\gamma^*p}^*(W^2, Q^2) + \sigma_{\gamma^*p}^T(W^2, Q^2) \\ &= \frac{\alpha R_{e^+e^-}}{3\pi} \sigma^{(\infty)}(W^2) \\ &\quad \times \left(I_T^{(1)} \left(\frac{\eta}{\rho}, \frac{\mu}{\rho} \right) G_T(u) \right. \\ &\quad \left. + I_L^{(1)}(\eta, \mu) G_L(u) \right), \end{aligned} \quad (3.1)$$

⁴ The photoabsorption cross section (3.1) and (3.2) in good approximation is determined by $\eta(W^2, Q^2)$, i.e. $\sigma_{\gamma^*p}(W^2, Q^2) \cong \sigma_{\rho^*p}(\eta(W^2, Q^2))$ except for a weak (logarithmic) W -dependence due to $\sigma^{(\infty)}(W^2)$ in (3.1) or $\sigma_{\gamma p}(W^2)$ in (3.2). The parameter ξ (not to be confused with ξ_L) is fixed at $\xi = \xi_0 = 130$, and for the range of $\eta(W^2, Q^2)$ of relevance for the present paper, one may put $\xi \rightarrow \infty$.

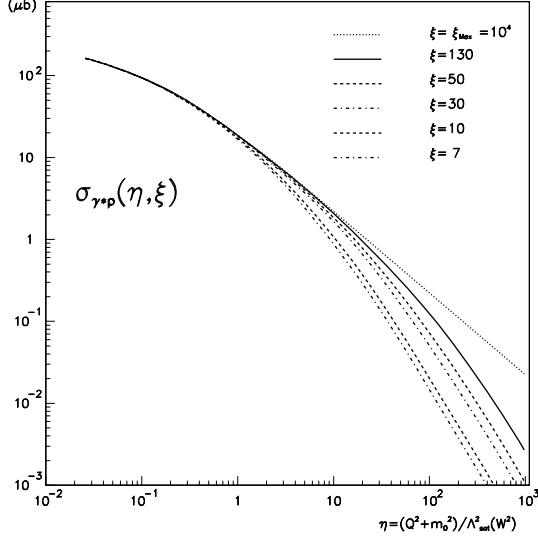


FIG. 1. The theoretical results for the photoabsorption cross section $\sigma_{\gamma^*p}(\eta(W^2, Q^2), \xi)$ in the CDP as a function of the low- x scaling variable $\eta(W^2, Q^2) = (Q^2 + m_0^2)/\Lambda_{sat}^2(W^2)$ for different values of the parameter ξ that determines the (squared) mass range $M_{q\bar{q}}^2 \leq m_1^2(W^2) = \xi \Lambda_{sat}^2(W^2)$ of the $\gamma^* \rightarrow q\bar{q}$ fluctuations that are taken into account. The experimental results for $\sigma_{\gamma^*p}(\eta(W^2, Q^2), \xi)$ lie on the full line corresponding to $\xi = \xi_0 = 130$, compare refs. [14, 15].

derived from an ansatz [13–15] for the W -dependent dipole cross section that essentially, via the structure of the coupling of the quark-antiquark state to two gluons, represents the color-gauge-invariant interaction of the $q\bar{q}$ dipole with the gluon-field in the nucleon. In (3.1), $R_{e^+e^-} = 3 \sum_q Q_q^2$, where q runs over the active quark flavors, and Q_q denotes the quark charge. The smooth transition to $Q^2 = 0$ photoproduction in (3.1) allows one [15] to replace (see (2.37) in ref. [15]) $\sigma^{(\infty)}(W^2)$, which stems from the normalization of the $(q\bar{q})$ proton dipole cross section, by the photoproduction cross section, and (3.1) becomes

$$\sigma_{\gamma^*p}(W^2, Q^2) = \frac{\sigma_{\gamma p}(W^2)}{\lim_{\eta \rightarrow \mu(W^2)} I_T^{(1)}\left(\frac{\eta}{\rho}, \frac{\mu(W^2)}{\rho}\right) G_T(u)} \times \left(I_T^{(1)}\left(\frac{\eta}{\rho}, \frac{\mu}{\rho}\right) G_T(u) + I_L^{(1)}(\eta, \mu) G_L(u) \right). \quad (3.2)$$

We note that $I_L^{(1)}(\eta, \mu)$ vanishes in the photoproduction $Q^2 = 0$ limit of $\eta(W^2, Q^2 = 0) = m_0^2/\Lambda_{sat}^2(W^2) \equiv \mu(W^2)$, and $G_T(u \equiv \frac{\xi}{\eta}) \simeq 1$, and for later reference we also note

$$\lim_{\eta \rightarrow \mu(W^2)} I_T^{(1)}\left(\frac{\eta}{\rho}, \frac{\mu(W^2)}{\rho}\right) = \ln \frac{\rho}{\mu(W^2)}. \quad (3.3)$$

For the general explicit analytic expressions for the functions $I_T^{(1)}\left(\frac{\eta}{\rho}, \frac{\mu(W^2)}{\rho}\right)$ and $I_L^{(1)}(\eta, \mu)$ we refer to Appendix

A. The functions $G_T\left(u \equiv \frac{\xi}{\eta}\right)$ and $G_L\left(u \equiv \frac{\xi}{\eta}\right)$ are given by

$$G_T(u) = \frac{2u^3 + 3u^2 + 3u}{2(1+u)^3} \simeq \begin{cases} \frac{3}{2} \frac{\xi}{\eta} & , \quad (\eta \gg \xi), \\ 1 - \frac{3}{2} \frac{\eta}{\xi} & , \quad (\eta \ll \xi), \end{cases} \quad (3.4)$$

and

$$G_L(u) = \frac{2u^3 + 6u^2}{2(1+u)^3} \simeq \begin{cases} 3 \left(\frac{\xi}{\eta}\right)^2 & , \quad (\eta \gg \xi), \\ 1 - 3 \left(\frac{\eta}{\xi}\right)^2 & , \quad (\eta \ll \xi), \end{cases} \quad (3.5)$$

where $u \equiv \xi/\eta$, and the constant parameter ξ restricts the masses of the contributing mass $q\bar{q}$ states via

$$M_{q\bar{q}}^2 \leq m_1^2(W^2) = \xi \Lambda_{sat}^2(W^2). \quad (3.6)$$

The numerical results for the photoabsorption cross section in Fig. 1 are obtained by numerical evaluation of (3.2) upon insertion of a $(\ln W^2)^2$ fit to the experimental results for the photoproduction cross section $\sigma_{\gamma p}(W^2)$ from the Particle Data Group [21]. The results in Fig. 1 were obtained for $W = 275$ GeV from

$$\sigma_{\gamma p}(W^2) = 0.003056 \left(34.71 + \frac{0.3894\pi}{M^2} \ln^2 \frac{W^2}{M_p^2 + M^2} \right) + 0.0128 \left(\frac{(M_p + M)^2}{W^2} \right)^{0.462}. \quad (3.7)$$

In (3.7), M_p denotes the proton mass, $M = 2.15$ GeV and $\sigma_{\gamma p}(W^2)$ is given in units of millibarn.

Before going into more detail, we note that the full curve in Fig. 1, which for the parameter ξ corresponds to the choice of $\xi = \xi_0 = 130$, provides a representation of the full set of experimental data on $\sigma_{\gamma^*p}(W^2, Q^2)$ at low $x \cong Q^2/W^2$, compare Fig. 8 in ref. [14].

In (3.1) and (3.2), the low- x scaling variable $\eta(W^2, Q^2)$ is given by

$$\eta \equiv \eta(W^2, Q^2) = \frac{Q^2 + m_0^2}{\Lambda_{sat}^2(W^2)}, \quad (3.8)$$

with

$$\mu \equiv \mu(W^2) = \eta(W^2, Q^2 = 0) = \frac{m_0^2}{\Lambda_{sat}^2(W^2)}, \quad (3.9)$$

the saturation scale, $\Lambda_{sat}^2(W^2)$, being parametrized by

$$\Lambda_{sat}^2(W^2) = C_1 \left(\frac{W^2}{1 \text{ GeV}^2} \right)^{C_2}, \quad (3.10)$$

and numerically, we have

$$m_0^2 = 0.15 \text{ GeV}^2, \quad C_1 = 0.31 \text{ GeV}^2; \quad C_2 = 0.27. \quad (3.11)$$

The parameter $\rho = \text{const}$ in (3.1) and (3.2) is related to the longitudinal-to-transverse ratio $R(W^2, Q^2)$ of the

photoabsorption cross section, and approximately we have $R(W^2, Q^2) \simeq 1/2\rho$ for $\eta(W^2, Q^2) \gg \mu(W^2)$, while $R(W^2, Q^2) = 0$ for $Q^2 = 0$. The total cross section $\sigma_{\gamma^*p}(W^2, Q^2)$ is fairly insensitive to the value of ρ for realistic values of ρ around $\rho \simeq 1$, and the evaluation presented in Fig. 1 is based on $\rho = \frac{4}{3}$.

In terms of the photoabsorption cross sections $\sigma_{\gamma_{L,T}^*p}(W^2, Q^2)$, in (3.1) and (3.2), the proton structure functions, relevant for the extraction of the gluon-density distribution, see (2.5), are given by

$$F_{L,T}(W^2, Q^2) = \frac{Q^2}{4\pi^2\alpha} \sigma_{\gamma_{L,T}^*p}(W^2, Q^2) \quad (3.12)$$

and

$$F_2(W^2, Q^2) = \frac{Q^2}{4\pi^2\alpha} \sigma_{\gamma^*p}(W^2, Q^2) = \frac{Q^2}{4\pi^2\alpha} (\sigma_{\gamma_T^*p}(W^2, Q^2) + \sigma_{\gamma_L^*p}(W^2, Q^2)). \quad (3.13)$$

Upon introducing the longitudinal-to-transverse ratio $R(W^2, Q^2)$ from (2.6), the longitudinal structure function becomes

$$F_L(W^2, Q^2) = \frac{R}{1+R} F_2(W^2, Q^2). \quad (3.14)$$

Explicitly, according to (3.2), we have

$$R(W^2, Q^2) = \frac{I_L^{(1)}(\eta, \mu) G_L(u)}{I_T^{(1)}\left(\frac{\eta}{\rho}, \frac{\mu}{\rho}\right) G_T(u)}. \quad (3.15)$$

For $Q^2 = 0$, as a consequence of electromagnetic gauge invariance,

$$R(W^2, Q^2 = 0) = 0, \quad (3.16)$$

while for $\eta(W^2, Q^2)$, restricted by the interval of $1 \ll \eta(W^2, Q^2) \ll \xi = \xi_0 = 130$ that will be of relevance subsequently, we have

$$R(W^2, Q^2) \approx \frac{1}{2\rho}, \quad (3.17)$$

with $\rho = \text{const}$ in the vicinity of $\rho \simeq 1$, and, accordingly, (3.14) becomes

$$F_L(W^2, Q^2) = \frac{1}{2\rho+1} F_2(W^2, Q^2), \quad (1 \ll \eta(W^2, Q^2) \ll \xi_0). \quad (3.18)$$

While (3.18) holds strictly for sufficiently large Q^2 , even for low values of Q^2 it may be used as an approximation, the vanishing of the longitudinal γ_L^*p interaction for $Q^2 \rightarrow 0$ being partly taken into account by the low- Q^2 limit of $F_2(W^2, Q^2)$ in (3.14).

For large Q^2 , specifically for $10\text{GeV}^2 \lesssim Q^2 \lesssim 100\text{GeV}^2$ the range of Q^2 of particular relevance in connection with pQCD, the experimental data on the proton structure

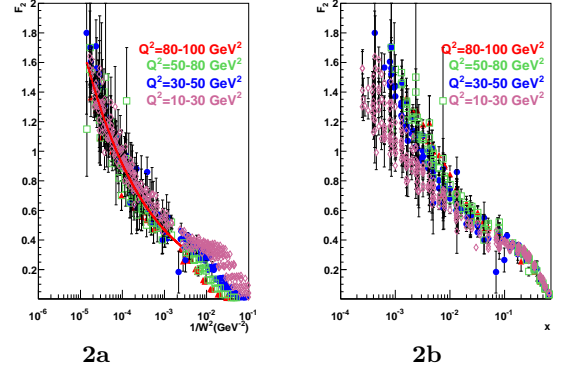


FIG. 2. In Fig.2a we show the experimental data for $F_2(x \simeq Q^2/W^2, Q^2)$ as a function of $1/W^2$, and in Fig.2b, for comparison, as a function of x . The theoretical prediction based on (3.19) with (3.20) is also shown in Fig.2a.

function $F_2(W^2, Q^2)$ in (3.13) depend on the single variable W^2 , compare Fig. 2 quoted from ref. [14].

A simple two-parameter eye-ball fit to the experimental data in Fig. 2 yields [14]

$$F_2(W^2) = f_2 \left(\frac{W^2}{1\text{GeV}^2} \right)^{C_2}, \quad (3.19)$$

where ⁵

$$f_2 = 0.063, \quad C_2 = 0.29. \quad (3.20)$$

The fit result is understood as a consequence of the CDP in the large- $\eta(W^2, Q^2)$ approximation. The structure function $F_2(W^2, Q^2)$ for $Q^2 \gg \Lambda_{sat}^2(W^2)$ according to (3.13) upon substitution of (3.1) takes the simple form

$$F_2(W^2, Q^2) = \frac{R_{e^+e^-} \sigma^{(\infty)}(W^2)}{24\pi^3} \frac{1+2\rho}{3} \Lambda_{sat}^2(W^2) \times \left(1 + 0 \left(\frac{1}{\eta} \right) \right). \quad (3.21)$$

Upon specifying $\Lambda_{sat}^2(W^2) = C_1 \left(\frac{W^2}{1\text{GeV}^2} \right)^{C_2}$ according to (3.10), the structure function (3.21) can directly be compared with (3.19),

$$F_2(W^2, Q^2) = \frac{R_{e^+e^-} \sigma^{(\infty)}(W^2)}{24\pi^3} \frac{1+2\rho}{3} C_1 \left(\frac{W^2}{1\text{GeV}^2} \right)^{C_2} \times \left(1 + 0 \left(\frac{1}{\eta} \right) \right) \equiv \hat{f}_2(W^2) \left(\frac{W^2}{1\text{GeV}^2} \right)^{C_2} \left(1 + 0 \left(\frac{1}{\eta} \right) \right). \quad (3.22)$$

⁵ The value of the exponent $C_2 = 0.29$ [20] agrees with the independent fit to the DIS experimental data based on the hard-Pomeron conjecture leading to the exponent $C_0 \simeq 0.30 \pm 0.1$.

The product $R_{e^+e^-}\sigma^{(\infty)}(W^2)$ is determined by the photoproduction cross section (3.7) according to

$$R_{e^+e^-}\sigma^{(\infty)}(W^2) = \frac{3\pi}{\alpha} \frac{\sigma_{\gamma p}(W^2)}{\ln \frac{\rho \Lambda_{sat}^2(W)}{m_0^2}}, \quad (3.23)$$

compare to (3.1) to (3.3).

For definiteness, in Table 1, we explicitly present the input for the evaluation of F_2 according to (3.22) that leads to

$$\hat{f}_2(W^2) = \begin{cases} 0.067 & , \text{ for } W^2 = 10^4 \text{ GeV}^2, \\ 0.068 & , \text{ for } W^2 = 10^5 \text{ GeV}^2. \end{cases} \quad (3.24)$$

TABLE I. The evaluation of $\hat{f}_2(W^2)$ defined by (3.22). The parameters ρ and m_0^2 in (3.22) and (3.23) are given by $\rho = 4/3$ and $m_0^2 = 0.15 \text{ GeV}^2$.

W^2 [GeV ²]	10 ⁴	10 ⁵
$\sigma_{\gamma p}$ [mb]	0.146	0.175
$\Lambda_{sat}^2(W^2) = C_1 \left(\frac{W^2}{1 \text{ GeV}^2} \right)^{C_2}$		
$C_1 = 0.31 \text{ GeV}^2$,	4.48	8.74
$C_2 = 0.29$		
$R_{e^+e^-}\sigma^{(\infty)}(W^2)$ [mb]	50.9	51.9
$\hat{f}_2(W^2)$	0.067	0.068

These values of $\hat{f}_2(W^2)$ are approximately 6 % to 7 % larger than the values from the eye-ball fit (3.19) in (3.20). The structure function $F_2(W^2, Q^2)$ is given by

$$F_2 \cong \begin{cases} 0.96 & , \text{ for } W^2 = 10^4 \text{ GeV}^2, \\ 1.91 & , \text{ for } W^2 = 10^5 \text{ GeV}^2. \end{cases} \quad (3.25)$$

For the determination of the gluon distribution according to (2.5), the structure functions in (3.12) and (3.13) have to be evaluated at a rescaled or shifted value of $x \rightarrow \xi_L x$, corresponding to a shift of $W^2 \rightarrow \xi_L^{-1} W^2$. In terms of the low-x scaling variable $\eta(W^2, Q^2)$, the shift becomes

$$\eta(W^2, Q^2) = \frac{Q^2 + m_0^2}{\Lambda_{sat}^2(W^2)} \rightarrow \frac{Q^2 + m_0^2}{\Lambda_{sat}^2(\xi_L^{-1} W^2)}. \quad (3.26)$$

For

$$\Lambda_{sat}^2(W^2) = C_1 \left(\frac{W^2}{1 \text{ GeV}^2} \right)^{C_2}, \quad (3.27)$$

to be employed subsequently, the shift becomes

$$\eta(W^2, Q^2) \rightarrow \xi_L^{C_2} \eta(W^2, Q^2). \quad (3.28)$$

The photoabsorption cross section (3.2) essentially only depends on $\eta(W^2, Q)$,

$$\sigma_{\gamma_{L,TP}}^*(W^2, Q^2) \cong \sigma_{\gamma_{L,TP}}^*(\eta(W^2, Q^2)), \quad (3.29)$$

since the $Q^2 = 0$ photoproduction factor in (3.2) depends only weakly on W^2 . The rescaling shift (3.28) applied to the cross section (3.2), accordingly, amounts to

$$\sigma_{\gamma_{L,TP}}^*(\eta(W^2, Q^2)) \rightarrow \sigma_{\gamma_{L,TP}}^*(\xi_L^{C_2} \eta(W^2, Q^2)). \quad (3.30)$$

Numerically, for $C_2 = 0.29$ and $\xi_L = 0.4$, we have

$$\xi_L^{C_2} \eta = 0.4^{0.29} \eta \cong 0.77 \eta(W^2, Q^2). \quad (3.31)$$

Explicitly, the gluon distribution (2.5) becomes

$$\alpha_s(Q^2) G(x, Q^2) = \frac{3\pi}{\sum_q Q_q^2} \frac{Q^2}{4\pi^2 \alpha} \sigma_{\gamma_{L,TP}}^*(\xi_L^{C_2} \eta(W^2, Q^2)). \quad (3.32)$$

The empirically verified low-x scaling of the photoabsorption cross section in the variable $\eta(W^2, Q^2)$ translates from the photoabsorption cross section to the gluon distribution divided by Q^2 . For sufficiently large Q^2 , with $\sigma_{\gamma_{L,TP}}^* \propto \Lambda_{sat}^2(W^2)/Q^2$, we obtain the asymptotic behavior of

$$\alpha_s(Q^2) G(x, Q^2) \propto \Lambda_{sat}^2(W^2). \quad (3.33)$$

The quantity $\Lambda_{sat}^2(W^2)$, also known as saturation scale, determines the gluon distribution function in the pQCD large- Q^2 limit.

IV. THE FROISSART-BOUNDED REPRESENTATION OF $F_2(x, Q)$.

In principle, any sufficiently accurate representation of the DIS electron-proton-scattering experimental data, relying on strict validity of the perturbative QCD improved parton model (pQCD), must lead to the same prediction of the gluon distribution function. Nevertheless, it appears illuminating to explicitly supplement results based on the CDP by results from an alternative representation of the DIS experimental data. In this spirit, we examine the precise fit to the experimental data by Block et al. [22]. The fit is based on a parametrization of the virtual-photon-proton cross section that saturates the $(\log W^2)^2$ bound derived from general principles for hadron-hadron cross sections by Froissart [23].

The results from DIS at low $x \leq 0.1$ and for a large range of Q^2 from $0.15 \text{ GeV}^2 \leq Q^2 \leq 3000 \text{ GeV}^2$ are represented by the structure function [22]

$$F_2(x, Q^2) = D(Q^2)(1-x)^n [C(Q^2) + A(Q^2) \ln \left(\frac{1}{x} \frac{Q^2}{Q^2 + \mu^2} \right) + B(Q^2) \ln^2 \left(\frac{1}{x} \frac{Q^2}{Q^2 + \mu^2} \right)]. \quad (4.1)$$

The power n and the scale μ^2 are given by $n = 11.49 \pm 0.99$ and $\mu^2 = 2.82 \pm 0.290 \text{ GeV}^2$. The logarithmic dependence on Q^2 of the functions $A(Q^2)$, $B(Q^2)$, $C(Q^2)$ and

$D(Q^2)$ is given in Appendix B and Table B1 reproducing Table II from ref. [22].

In distinction from the CDP, the Froissart-bounded fit does not explicitly provide a representation of the longitudinal-to-transverse ratio R . When deducing the gluon distribution function, the value of R from the CDP will have to be adopted.

V. THE RESULTS FOR THE GLUON DISTRIBUTION FUNCTION.

We turn to the numerical results for the gluon distribution which follow from the evaluation of (2.5) upon substitution of the representation of the DIS experimental results in the CDP and the Froissart-bounded representation, as given in Sections 3 and 4, respectively.

Substitution into (2.5) of the results (3.12) with (3.2) for $F_L(W^2, Q^2)$ yields

$$\alpha_s(Q^2)G(x, Q^2) = \frac{3\pi}{\sum_q Q_q^2} F_L(\xi_L x, Q^2) = \frac{9Q^2}{4\pi\alpha R_{e^+e^-}} \times \left(\frac{\sigma_{\gamma p}(W^2)}{\left(\ln \frac{\rho}{\mu}\right) G_T\left(\frac{\xi}{\eta}\right)} I_L^{(1)}(\eta, \mu) G_L\left(\frac{\xi}{\eta}\right) \right) \Big|_{W^2 \rightarrow \xi_L^{-1} W^2} \quad (5.1)$$

The variables $\eta = \eta(W^2, Q^2)$ and $\mu(W^2)$ are given by (see (3.8), (3.9)),

$$\eta(W^2, Q^2) = \frac{Q^2 + m_0^2}{\Lambda_{sat}^2(W^2)}, \quad \mu(W^2) = \frac{m_0^2}{\Lambda_{sat}^2(W^2)}, \quad (5.2)$$

where

$$\Lambda_{sat}^2(W^2) = C_1(W^2)^{C_2} = 0.31 \left(\frac{W^2}{1\text{GeV}^2} \right)^{0.29} \text{GeV}^2, \quad (5.3)$$

with $C_2 = 0.29$ from (3.20) and

$$m_0^2 = 0.15 \text{ GeV}^2. \quad (5.4)$$

For the assumed four numbers of flavors,

$$R_{e^+e^-} \equiv 3 \sum_q Q_q^2 = \frac{10}{3}. \quad (5.5)$$

The parameter ρ , denoting the size enhancement of transversely relative to longitudinally polarized $q\bar{q}$ fluctuations, is given by

$$\rho = \frac{4}{3}. \quad (5.6)$$

The parameter ξ , that stands for the upper limit, $\xi \Lambda_{sat}^2(W^2)$, of masses of $q\bar{q}$ fluctuations actively contributing, is given by $\xi = 130$. At the relevant (low)

values of $\eta(W^2, Q^2)$, the limit of $\xi \rightarrow \infty$ and $G_T\left(\frac{\xi}{\eta}\right) = G_L\left(\frac{\xi}{\eta}\right) = 1$ (see (3.4) and (3.5)) may be taken without loss of generality, compare Fig. 1. The $\log(W^2)$ fit to the photoproduction experimental results is given by (3.7), and, finally, the shift factor ξ_L according to (2.4) is given by

$$\xi_L = 0.4. \quad (5.7)$$

The essential effect of the shift $W^2 \rightarrow \xi_L^{-1} W^2$, in (5.1) amounts to

$$\eta(W^2, Q^2) \rightarrow \xi_L^{C_2} \eta(W^2, Q^2), \quad (5.8)$$

compare (3.30), the $Q^2 = 0$ photoproduction term in (5.1), including its normalization by the denominator in (5.1), being hardly affected due to its weak dependence on W^2 .

According to (2.5), the gluon distribution may equivalently be expressed in terms of the structure function $F_2(\xi_L x, Q^2)$ instead of $F_L(\xi_L x, Q^2)$, together with the longitudinal-to-transverse ratio R . For sufficiently large Q^2 , according to (2.5) and (3.18), with $R = 1/2\rho$,

$$\alpha_s(Q^2)G(x, Q^2) = \frac{9\pi}{R_{e^+e^-}} \frac{1}{2\rho + 1} F_2(\xi_L x, Q^2). \quad (5.9)$$

As noted in connection with (3.18), representation (5.9), at small Q^2 may be used as an approximation of the gluon distribution.

For Q^2 sufficiently large, specifically for $20 \text{ GeV}^2 \lesssim Q^2 \lesssim 100 \text{ GeV}^2$, the large- Q^2 limit of (5.1) given by (3.19) becomes relevant. It implies the simple large- Q^2 representation of

$$\alpha_s(Q^2)G(x, Q^2) = \frac{9\pi}{R_{e^+e^-}} \frac{1}{(2\rho + 1)} F_2(\xi_L x, Q^2) = \frac{9\pi}{R_{e^+e^-}} \frac{1}{(2\rho + 1)} f_2 \xi_L^{-0.29} \left(\frac{W^2}{1\text{GeV}^2} \right)^{C_2=0.29}, \quad (5.10)$$

where $f_2 = 0.063$, and $\rho = \frac{4}{3}$.

In Fig. 3, we show the gluon distribution deduced from $F_L(W^2, Q^2)$ according to (5.1) as a function of W^2 for various values of Q^2 , where $1\text{GeV}^2 \leq Q^2 \leq 100\text{GeV}^2$. The results in Fig. 3, for Q^2 sufficiently above $Q^2 \cong 10 \text{ GeV}^2$, indeed converge towards the asymptotic representation (5.10).

The results in Fig. 4, for $1\text{GeV}^2 \leq Q^2 \leq 10\text{GeV}^2$ compared with the results in Fig. 3, show the expected increase of the gluon distribution resulting from employing the large- Q^2 approximation (5.9). For sufficiently large Q^2 , the results in Fig. 4, based on $F_2(\xi_L x, Q^2)$ according to (5.9), coincide with the ones in Fig. 3 based on $F_L(\xi_L x, Q^2)$ according to (5.1).

For Figs. 5 and 6, the energy variable, W , of the CDP is replaced by $x \simeq Q^2/W^2$. The increase of x for

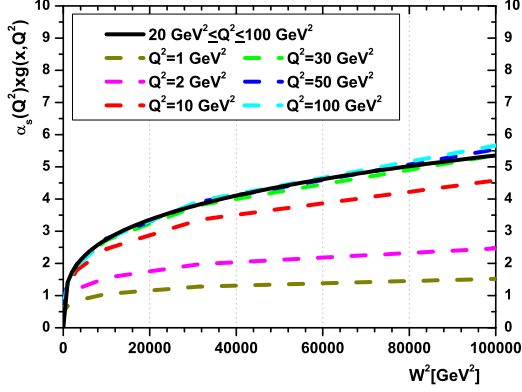


FIG. 3. The gluon distribution $\alpha_s(Q^2)xg(x, Q^2) \equiv \alpha_s(Q^2)G(x, Q^2)$ of the CDP, compare (5.1), as a function of W^2 for various values of Q^2 . The solid line shows the asymptotic limit (5.10) that is reached at $Q^2 \gtrsim 30\text{GeV}^2$.

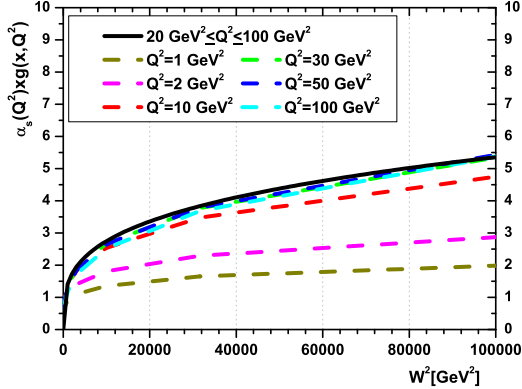


FIG. 4. As Fig. 3, but based on (5.9), employing $R = \text{const} = 1/2\rho = 3/8$. Compare text for details.

$Q^2 = 1.9 \text{ GeV}^2$ in the range of $10^{-4} \leq x \leq 10^{-1}$ corresponds to an increase of $\eta(W^2, Q^2 = 1.9 \text{ GeV}^2)$ according to $0.35 \leq \eta \leq 2.6$, with W^2 decreasing according to $1.9 \times 10^4 \text{ GeV}^2 \geq W^2 \geq 19 \text{ GeV}^2$. Taking into account the proportionality of the gluon distribution to the photoabsorption cross section (3.32), and consulting the results in Fig. 1, we expect a (hadronlike) increase of the gluon distribution by a factor of about 3.5 with decreasing x in the interval $10^{-1} \geq x \geq 10^{-4}$.

Multiplication of the results in Fig. 5 by $\alpha_s(Q^2 = 1.9 \text{ GeV}^2)^{-1} = 0.480^{-1} = 2.083$ yields the results for $xg(x, Q^2) \equiv G(x, Q^2)$ that are shown in

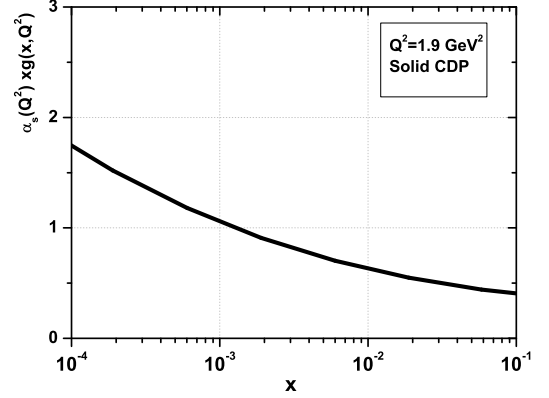


FIG. 5. The gluon-distribution function $\alpha_s(Q^2)xg(x, Q^2)$ of the CDP as a function of $x \cong Q^2/W^2$ at the (low) value of $Q^2 = 1.9 \text{ GeV}^2$, the scale frequently used as input scale [6].

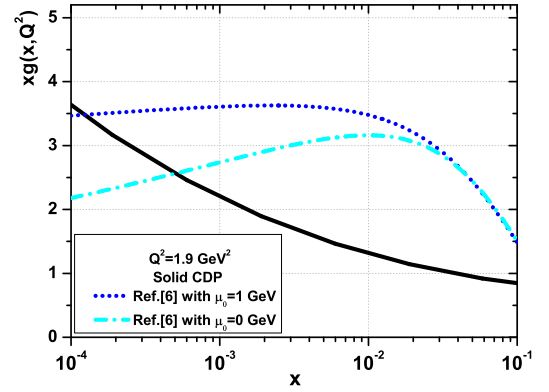


FIG. 6. As Fig. 5, but for $xg(x, Q^2)$ instead of $\alpha_s(Q^2)xg(x, Q^2)$. The CDP results are compared with the results from ref. [6]

Fig. 6⁶

In Fig. 6, we compare with the results obtained in ref. [6] upon introducing absorptive corrections to the measured proton structure functions, and a modification of $\alpha_s(Q^2)$ by $\alpha_s(Q^2 + \mu_0^2)$. The gluon distributions from ref. [6] in Fig. 6 are given by [6]

$$\begin{aligned} xg(x) &= 5.63x^{0.103}(1-x)^{10.261} \text{ for } \mu_0 = 0 \text{ GeV}, \\ xg(x) &= 4.21x^{0.021}(1-x)^{9.427} \text{ for } \mu_0 = 1 \text{ GeV}. \end{aligned} \quad (5.11)$$

As seen in Fig. 6, the results from ref. [6] are dramatically different from ours. The results obtained by

⁶ The value of $\alpha_s(Q^2 = 1.9 \text{ GeV}^2) = 0.480$ is obtained for $\Lambda_{QCD} = 437 \text{ MeV}$ corresponding to $\alpha_s(M_Z^2) = 0.118$.

exploiting the smooth low- Q^2 transition of the CDP in the pQCD-improved parton model do not support the necessity of modifications by absorptive effects. For further discussions on the reliability of our approach of incorporating the CDP representation into pQCD, see sections VI and VII.

The analysis of the gluon distribution function that led to the results in Figs. 3 to 6 is based on the representation of the proton structure function in the CDP. We expect that other precise and theoretically well-founded representations of the measured structure functions will lead to (at least approximately) identical results for the gluon distribution. Explicitly this equivalence is tested by the example of employing the fit to the proton structure function in the Froissart-bounded representation⁷ from ref. [22], described in Section IV.

Since the theoretical representation in this approach does not isolate the longitudinal structure function, the gluon distribution must be deduced from $F_2(\xi_L x, Q^2)$ with $\rho = \frac{4}{3}$ in (5.9).

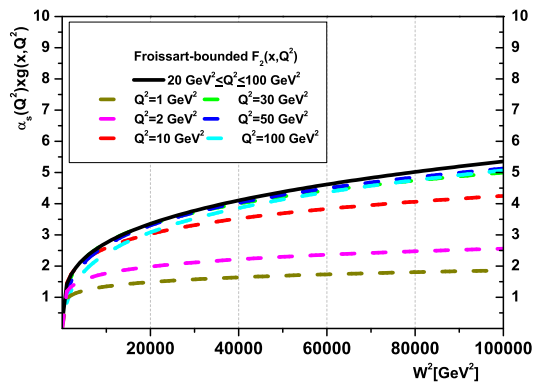


FIG. 7. The gluon distribution $\alpha_s(Q^2)xg(x, Q^2)$ deduced from the Froissart-bounded representation of the proton structure function $F_2(x, Q^2)$ given in ref. [22]

The results in Fig. 7 for large Q^2 , asymptotically, agree with the CDP result. For $Q^2 \lesssim 10 \text{ GeV}^2$, there are acceptable deviations, seen upon comparing the results in Fig. 7 with the ones in Figs. 3 and 4.

In Figs. 8 and 9, respectively, we present the comparison of the gluon distribution from the Froissart-bounded representation of $F_2(x, Q^2)$ with the results based on the CDP, and with the results from ref. [6] at $Q^2 = 1.9 \text{ GeV}^2$ based on pQCD modified by power law corrections and

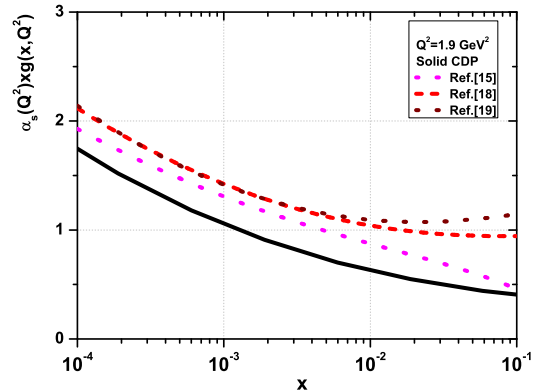


FIG. 8. The gluon-distribution function $\alpha_s(Q^2)xg(x, Q^2)$ as a function of $x \cong Q^2/W^2$ at $Q^2 = 1.9 \text{ GeV}^2$ from the CDP, and from Froissart-bounded representations in refs. [22], [24] and [25].

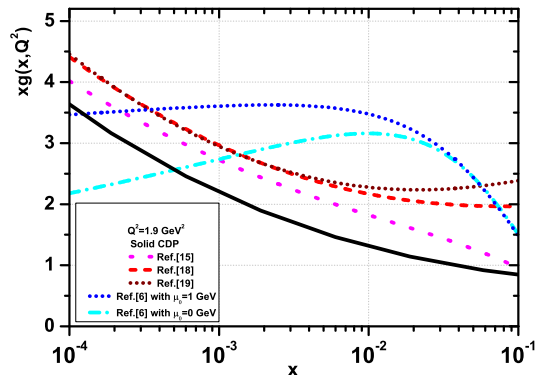


FIG. 9. Same as Fig. 8 except for showing $xg(x, Q^2)$ instead of $\alpha_s(Q^2)xg(x, Q^2)$. The CDP results and the results from the Froissart-bounded representation are compared with the results from ref. [6].

absorptive effects. In addition to the results extracted from the fit [22] to the proton structure function described in Section IV., in Figs. 8 and 9, we have employed two additional somewhat different fits from refs. [24, 25] without entering into a detailed description of these fits.

By comparison of the results on the gluon distribution based on the representation of the body of DIS experimental data of the proton structure functions in the CDP, and in the Froissart-bounded approach, at $Q^2 = 1.9 \text{ GeV}^2$, we find a consistent behavior as expected.

⁷ We evaluate the gluon distribution from the pQCD approximation (2.5) as well as (6.14) below, in distinction from the approach in ref. [22] that is based on an exact determination of $G(x, Q^2)$ [24] upon converting (6.10) below into an inhomogeneous second order differential equation for $G(x, Q^2)$.

VI. THE CONSISTENCY OF PQCD AND CDP.

The results on the gluon distribution of the CDP in Section V. are obtained by assuming validity of the approximate pQCD representations (2.1), (2.4) and (2.5) upon substitution of the longitudinal structure function of the proton from the CDP. In the present section, we examine the validity of this assumption.

In the pQCD improved parton model, the proton structure function $F_L(x, Q^2)$ to lowest order of $\alpha_s(Q^2)$ is given by [19]

$$F_L(x, Q^2) = \frac{\alpha_s(Q^2)}{4\pi} \left(\frac{16}{3} I_F + 8 \sum Q_q^2 I_g \right), \quad (6.1)$$

where

$$I_F \equiv I_F(x, Q^2) = \int_x^1 \frac{dy}{y} \left(\frac{x}{y} \right)^2 F_2(y, Q^2), \quad (6.2)$$

and

$$I_g \equiv I_g(x, Q^2) = \int_x^1 \frac{dy}{y} \left(\frac{x}{y} \right)^2 \left(1 - \frac{x}{y} \right) G(y, Q^2), \quad (6.3)$$

and $\sum Q_q^2 = 10/9$ for four flavors of quarks. The term proportional to I_F in (6.1) is due to γ^* -quark (antiquark) interaction with gluon emission,

$$\gamma^* + q(\bar{q}) \rightarrow q(\bar{q}) + g, \quad (6.4)$$

while the term proportional to I_g in (6.1) originates from quark-antiquark production,

$$\gamma^* + g \rightarrow q\bar{q}. \quad (6.5)$$

The successful representation of the data on DIS in the CDP is based on incorporating [12] the $q\bar{q}$ -color-dipole interaction with the gluon field of the proton, ($\gamma^* \rightarrow q\bar{q}$) + $g \rightarrow q\bar{q}$ into the mass-dispersion relation of Generalized Vector Dominance (GVD) [16]. Accordingly, we expect that the gluon term associated with reaction (6.5) will be the dominant one in (6.1). We appropriately rewrite (6.1) as

$$F_L(x, Q^2) \left(1 - \frac{4\alpha_s(Q^2)}{3\pi} (2\rho + 1) \frac{I_F(x, Q^2)}{F_2(x, Q^2)} \right) = \frac{2\alpha_s(Q^2)}{\pi} \sum_q Q_q^2 I_g(x, Q^2), \quad (6.6)$$

where the large- Q^2 representation of $F_L = (1/(2\rho + 1)) F_2$ from (3.18) was inserted. For sufficiently large $Q^2 \gg \Lambda_{sat}^2(W^2)$, according to (3.21),

$$F_2 \left(W^2 = \frac{Q^2}{x}, Q^2 \right) \propto \Lambda_{sat}^2 \left(W^2 = \frac{Q^2}{x} \right) \propto \left(\frac{Q^2}{x} \right)^{C_2}. \quad (6.7)$$

Evaluating the integral $I_F(x, Q^2)$ in (6.2) for $F_2 \left(W^2 = \frac{Q^2}{x}, Q^2 \right)$ in (6.7)⁸, the ratio I_F/F_2 in (6.6) is found to be given by

$$\frac{I_F}{F_2} = \frac{1}{2 + C_2}. \quad (6.8)$$

Numerically, with $C_2 = 0.29$, $\rho = 4/3$ and $\alpha_s(Q^2) \cong 0.1$, we find that $F_L(x, Q^2)$ in (6.6) becomes

$$F_L(x, Q^2) \cong \frac{2\alpha_s(Q^2)}{\pi} \sum_q Q_q^2 I_g(x, Q^2) (1 + 0.07). \quad (6.9)$$

The proton structure, $F_L(x, Q^2)$, from the CDP, interpreted within the pQCD improved parton model, is indeed dominantly determined by the gluon distribution of the proton. The CDP predicts that the photon dominantly interacts with quark-antiquark pairs originating from gluons. According to (6.9), using the approximation (2.1) of the representation (6.1) to determine the gluon distribution of the CDP is justified at the level of about 7 %.

The fluctuation of the photon to on-shell $q\bar{q}$ states, $\gamma^* \rightarrow q\bar{q}$, from GVD and the CDP, with subsequent interaction of the $q\bar{q}$ states with gluons in the proton, in the pQCD improved parton model appears as fluctuation of the gluon into $q\bar{q}$ pairs with subsequent interaction of the $q\bar{q}$ pairs with the photon.

Having established the reliability of (2.1), we turn to examining the reliability of the approximation (2.4) of replacing the integral over the gluon distribution (2.2) and (6.3) by the rescaling shift $x \rightarrow \xi_L x$ or $W^2 \rightarrow \xi_L^{-1} W^2$, according to (2.4), as employed in the determination of the gluon distribution according to (5.1).

TABLE II. The Table shows the ratio of $F_L(W^2, Q^2)$ from pQCD according to (2.1) upon substitution of (2.5), to $F_L(W^2, Q^2)$ from (3.12) with (3.2). Compare text for more detail.

	$W^2 = 10^5$ [GeV ²]	$W^2 = 10^4$ [GeV ²]	$W^2 = 10^3$ [GeV ²]
$Q^2 = 100$ [GeV ²]	1.043	1.037	0.981
$Q^2 = 50$ [GeV ²]	1.041	1.037	1.012
$Q^2 = 10$ [GeV ²]	1.035	1.035	1.030
$Q^2 = 1$ [GeV ²]	1.015	1.021	1.026

⁸ We assume $\sigma^{(\infty)}(W^2) \cong const$, i.e. we are ignoring the weak additional W dependence in (3.21).

In Table II, we show the ratio of the structure function $F_L(W^2, Q^2)$, thus obtained from (2.1) upon insertion of (2.5) into (2.2), to the CDP structure function $F_L(W^2, Q^2)$ in (3.12) with (3.2) that was used as input in evaluating the scaling-shift formula (5.1) identical to (2.5). The deviations of this ratio from unity is below 5 %. The determination of the gluon distribution function by replacing the original pQCD result (2.1) by the approximation (2.5) is indeed a reliable one.

The Q^2 dependence of the gluon distribution function according to (5.1) and (5.9) is determined by the Q^2 dependence of the proton structure functions in the CDP. In the last part of this Section, we examine the consistency of the Q^2 dependence thus obtained for the gluon distribution from the CDP, with the Q^2 dependence predicted from pQCD. To order $\alpha_s(Q^2)$, only processes (6.4) and (6.5) contribute, and accordingly we can restrict ourselves to investigating the consistency of the Q^2 dependence from the CDP with the Q^2 dependence from the first DGLAP evolution equation [9].

The change of $F_2(x, Q^2)$ with Q^2 , its evolution is given by [9]

$$\frac{\partial}{\partial \ln Q^2} F_2(x, Q^2) = \frac{\alpha_s(Q^2)}{2\pi} \int_x^1 dz P_{qq}(z) F_2\left(\frac{x}{z}, Q^2\right) + \frac{R_{e^+e^-}}{3\pi} \int_0^{1-x} dz P_{qg}(z) G\left(\frac{x}{1-z}, Q^2\right), \quad (6.10)$$

where

$$P_{qq}(z) = \frac{4}{3} \left(\frac{1+x^2}{(1-x)_+} + \frac{3}{2} \delta(1-x) \right), \quad (6.11)$$

and

$$P_{qg}(z) = \frac{1}{2} (z^2 + (1-z)^2). \quad (6.12)$$

Motivated by the previous result that the proton structure functions are dominated by the $g \rightarrow q\bar{q}$ transition (6.5), we assume that this dominance also holds for the derivative of $F_2(x, Q^2)$ in (6.10). Rewriting (6.10) as

$$\begin{aligned} & \frac{\partial F_2(x, Q^2)}{\partial \ln Q^2} \left(1 - \frac{\int_x^1 dz P_{qq}(z) F_2\left(\frac{x}{z}, Q^2\right)}{\frac{\partial}{\partial \ln Q^2} F_2(x, Q^2)} \right) \\ &= \frac{R_{e^+e^-}}{3\pi} \int_0^{1-x} dz P_{qg}(z) G\left(\frac{x}{1-z}, Q^2\right), \end{aligned} \quad (6.13)$$

we put the additive term next to unity in (6.13) to zero, referring to the numerical analysis at the end of this section, and consider the remaining term in (6.13) that contains the gluon distribution function.

Exploiting the symmetry of $P_{qg}(z)$ in (6.12) around $z = 1/2$, the first derivative of $G(x/(1-z), Q^2)$ in a Taylor expansion of $G(x/(1-z), Q^2)$ around $z = \frac{1}{2}$, yields a vanishing contribution to the integral in (6.13), and approximately [26]

$$\frac{\partial F_2(x, Q^2)}{\partial \ln Q^2} = \frac{R_{e^+e^-}}{9\pi} \alpha_s(Q^2) G\left(\frac{x}{\xi_2}, Q^2\right). \quad (6.14)$$

with $x/\xi_2 = 2x$, or $\xi_2 = 1/2$. Replacing the gluon distribution in (6.14) by its proportionality (2.5) to the structure function $F_2(x, Q^2)$, (6.14) becomes

$$\frac{\partial F_2(x, Q^2)}{\partial \ln Q^2} = F_L\left(\frac{\xi_L}{\xi_2} x, Q^2\right) = \frac{1}{2\rho+1} F_2\left(\frac{\xi_L}{\xi_2} x, Q^2\right). \quad (6.15)$$

So far no specific ansatz for the proton structure function was used. Introducing the large- Q^2 power-law of the CDP (3.21) with (3.10),

$$F_2(x, Q^2) \sim (W^2)^{C_2} = \left(\frac{Q^2}{x}\right)^{C_2}, \quad (6.16)$$

from (6.15) we obtain the important constraint

$$C_2 \left(\frac{Q^2}{x}\right)^{C_2} = \frac{1}{2\rho+1} \left(\frac{Q^2}{x}\right)^{C_2} \left(\frac{\xi_2}{\xi_L}\right)^{C_2}, \quad (6.17)$$

or

$$C_2(2\rho+1) \left(\frac{\xi_L}{\xi_2}\right)^{C_2} = 1. \quad (6.18)$$

Expansion of the exponential to first order in C_2 yields the convenient expression for C_2 ,

$$C_2 \cong \frac{1}{2\rho+1} \frac{1}{\left(1 - \frac{1}{2\rho+1} \ln \frac{\xi_2}{\xi_L}\right)}. \quad (6.19)$$

For $\xi_2/\xi_L = 0.5/0.4 = 1.25$, with $\rho = \frac{4}{3}$, one finds $C_2 \cong 0.29$ for the exponent C_2 in (6.18).

The prediction of $C_2 \cong 0.29$ is based on the assumption that the evolution in Q^2 is entirely due to $q\bar{q}$ pairs originating from gluons $g \rightarrow q\bar{q}$, see (6.13) and (6.14). The agreement of the prediction for C_2 with the experimentally determined value, given in (3.20), provides empirical evidence for, or confirms the approximation of reducing the complete evolution equation (6.13) to its reduced form employed in (6.14). The incoming photon essentially only interacts with $q\bar{q}$ pairs originating from the $g \rightarrow q\bar{q}$ transition.

Coming back to (6.13), we briefly estimate the magnitude of the neglected additive term next to unity on the left-hand side in (6.13). With the proportionality of $F_2(W^2, Q^2)$ to $\Lambda_{sat}^2(W^2 = Q^2/x) \sim (Q^2/x)^{C_2}$, the ratio in (6.13) becomes

$$\frac{1}{C_2} \frac{\alpha_s(Q^2)}{2\pi} \int_x^1 dy P_{qq}(y) y^{C_2}. \quad (6.20)$$

Evaluation of the integral upon substitution of $P_{qq}(z)$ from (6.11) implies

$$- \frac{1}{C_2} \frac{\alpha_s(Q^2)}{2\pi} \int_x^1 dy P_{qq}(y) y^{C_2} = \frac{0.0205}{0.29} \cong 0.07. \quad (6.21)$$

Introducing the notation $\Delta = 0.07$, according to (6.21), the evolution equation (6.13) becomes

$$\frac{\partial}{\partial \ln Q^2} F_2(x, Q^2) \cong \frac{R_{e^+e^-}}{3\pi} \int_0^{1-x} dz P_{qg}(z) G\left(\frac{x}{1-z}, Q^2\right) \times (1 - \Delta). \quad (6.22)$$

Evaluation of the integral in (6.22) for $G(x, Q^2) \sim \Lambda_{sat}^2(Q^2/\xi_L x)^{C_2}$ yields a factor of

$$\frac{2}{3} \left(\frac{1}{2}\right)^{C_2} = 0.5453, \quad (6.23)$$

if the Taylor expansion is used for $G\left(\frac{x}{1-z}, Q^2\right)$, to be compared with the exact evaluation,

$$\frac{2}{(3 + C_2)(2 + C_2)(1 + C_2)} + \frac{1}{3 + C_2} = 0.5097. \quad (6.24)$$

The error induced by substituting the approximation (6.23) amounts to $1 - \Delta' = 1 - 0.07$. The total error induced by putting $\Delta = \Delta' = 0$ in (6.22) amounts to $(1 - \Delta)^2 \cong 0.86$, or about 14 %.

We conclude: the CDP with the power-law ansatz of $F_2(x, Q^2) \sim (Q^2/x)^{C_2}$ for large Q^2 fulfills evolution with Q^2 at large Q^2 and implies the empirically successful prediction of $C_2 \cong 0.29$.

VII. EVOLUTION AT LOW $Q^2 \gtrsim 1.9\text{GeV}^2$.

In considering the validity of the pQCD evolution equation (6.10) for $F_2(x, Q^2)$, we so far restricted ourselves to large values of Q^2 , sufficiently large with respect to $\Lambda_{sat}^2(W^2)$, effectively, $Q^2 \gtrsim 10\text{GeV}^2$ to 20GeV^2 . Employing the large- Q^2 -representation for $F_2(x, Q^2) \sim \left(\frac{Q^2}{x}\right)^{C_2}$, the validity of the evolution equation (6.10) implied the restriction (6.18) that predicts the exponent C_2 in $\Lambda_{sat}^2(W^2) \sim (W^2)^{C_2}$ from the transverse- $q\bar{q}$ -size parameter ρ , where ρ has the preferred value of $\rho = 4/3$.

In the present Section, we lift the restriction on the size of Q^2 by allowing for values of Q^2 as low as $Q^2 \gtrsim 1.9\text{GeV}^2$, the value frequently adopted when applying pQCD to electron-proton DIS.

The proton structure functions entering (6.15) according to (3.1), (3.2) and (3.12) are given by

$$F_2(x, Q^2) \equiv F_2\left(\eta\left(W^2 = \frac{Q^2}{x}, Q^2\right), \mu\left(W^2 = \frac{Q^2}{x}\right), W^2 = \frac{Q^2}{x}\right) \quad (7.1)$$

$$= \frac{Q^2}{4\pi^2\alpha \ln \frac{\rho}{\mu(W^2)}} \left(I_T^{(1)}\left(\frac{\eta}{\rho}, \frac{\mu}{\rho}\right) G_T(u) + I_L^{(1)}(\eta, \mu) G_L(u) \right),$$

and

$$F_L(x, Q^2) \equiv F_L\left(\eta\left(W^2 = \frac{Q^2}{x}, Q^2\right), \mu\left(W^2 = \frac{Q^2}{x}\right), W^2 = \frac{Q^2}{x}, Q^2\right) = \frac{Q^2}{4\pi^2\alpha \ln \frac{\rho}{\mu(W^2)}} I_L^{(1)} G_L(u). \quad (7.2)$$

The fit to the experimental data of $\sigma_{\gamma p}(W^2)$ is given by (3.7). For the explicit expressions for $I_T^{(1)}$ and $I_L^{(1)}$ in (7.1) and (7.2), we refer to Appendix A. In the present context we can restrict ourselves to the range of $\eta \ll \xi = 130$, and accordingly $G_{L,T}(u) = 1$ in (7.1) and (7.2), see (3.4) and (3.5).

Adopting (3.10),

$$\Lambda_{sat}^2(W^2) = C_1 \left(\frac{W^2}{1\text{GeV}^2} \right)^{C_2}, \quad W^2 = \frac{Q^2}{x}, \quad (7.3)$$

$\eta(W^2, Q^2)$ from (3.8) expressed in terms of the parton variables x and Q^2 becomes

$$\eta \equiv \eta(W^2, Q^2) = \frac{x^{C_2}}{C_1} \frac{(Q^2 + m_0^2)}{(Q^2)^{C_2}}, \quad (7.4)$$

and $\mu(W^2)$ from (3.9) is given by

$$\mu \equiv \mu(W^2) = \frac{x^{C_2}}{C_1} \frac{m_0^2}{(Q^2)^{C_2}}. \quad (7.5)$$

The numerical value of the exponent C_2 , for a given value of ρ is fixed by the constraint (6.18).

Turning to the examination of the validity of the evolution equation for $F_2(x, Q^2)$ in the form of the first equality in (6.15), we introduce the ratio

$$\text{Ratio} \equiv \frac{\frac{\partial F_2(x, Q^2)}{\partial \ln Q^2}}{F_L\left(\frac{\xi_L}{\xi_2} x, Q^2\right)} \quad (7.6)$$

$$= 1 + \Delta \left(\eta\left(W^2 = \frac{Q^2}{x}, Q^2\right), \mu\left(W^2 = \frac{Q^2}{x}\right) \right),$$

where, according to the validity of (6.15) under constraint (6.18), we have $\Delta(\eta, \mu) \cong 0$ for sufficiently large $Q^2 \gtrsim 10\text{GeV}^2$. Deviations from the validity of the evolution equation are accordingly parametrized by $\Delta(\eta, \mu)$ according to (7.6).

From (7.1), the derivative of $F_2(x, Q^2)$ is obtained as

$$\frac{\partial F_2(x, Q^2)}{\partial \ln Q^2} = \frac{Q^2}{4\pi^2\alpha \ln \frac{\rho}{\mu(W^2)}} \left[\left(I_T^{(1)}\left(\frac{\eta}{\rho}, \frac{\mu}{\rho}\right) + I_L^{(1)}(\eta, \mu) \right) \times \left(1 + \frac{\ln \frac{\rho}{\mu(W^2)}}{\sigma_{\gamma p}(W^2)} \frac{\partial}{\partial \ln W^2} \frac{\sigma_{\gamma p}(W^2)}{\ln \frac{\rho}{\mu(W^2)}} \right) + \frac{\partial}{\partial \ln Q^2} \left(I_T^{(1)}\left(\frac{\eta}{\rho}, \frac{\mu}{\rho}\right) + I_L^{(1)}(\eta, \mu) \right) \right], \quad (7.7)$$

and the denominator of (7.6) is given by

$$F_L\left(\frac{\xi_L}{\xi_2}x, Q^2\right) = \frac{Q^2}{4\pi^2\alpha} \frac{\sigma_{\gamma p}\left(\frac{\xi_2}{\xi_L}W^2\right)}{\ln\frac{\rho}{\mu\left(\frac{\xi_2}{\xi_L}W^2\right)}} I_L^{(1)}\left(\frac{\xi_L}{\xi_2}\eta, \frac{\xi_L}{\xi_2}\mu\right). \quad (7.8)$$

In connection with the derivatives appearing in (7.7), we mention the equality $\frac{\partial}{\partial \ln W^2} = \frac{\partial}{\partial \ln Q^2}$, and moreover, we note the derivatives

$$\begin{aligned} Q^2 \frac{\partial \eta}{\partial Q^2} &= (1 - C_2)\eta - \mu \\ Q^2 \frac{\partial \mu}{\partial Q^2} &= -C_2\mu. \end{aligned} \quad (7.9)$$

Noting that $\sigma_{\gamma p}(W^2)$ only weakly depends on W^2 , one may approximate “Ratio” defined in (7.6) by ignoring the derivative of $\sigma_{\gamma p}(W^2)$ in (7.7). Explicitly, Ratio from (7.6) becomes⁹

$$\begin{aligned} \text{Ratio} &= \frac{1}{I_L^{(1)}\left(\frac{\xi_L}{\xi_2}, \frac{\xi_L}{\xi_2}\mu\right)} \\ &\times \left[I_T^{(1)}\left(\frac{\eta}{\rho}, \frac{\mu}{\rho}\right) + I_L^{(1)}(\eta, \mu) \right. \\ &\left. + \frac{\partial}{\partial \ln Q^2} \left(I_T^{(1)}\left(\frac{\eta}{\rho}, \frac{\mu}{\rho}\right) + I_L^{(1)}(\eta, \mu) \right) \right]. \end{aligned} \quad (7.10)$$

Moreover, since $\mu(W^2) = m_0^2/\Lambda_{sat}^2(W^2)$, with $m_0^2 = 0.15\text{GeV}^2$, for sufficiently large W^2 , $\mu(W^2)$ is small compared to unity, $\mu(W^2) \ll 1$, and the approximation of $I_L^{(1)}$ and $I_T^{(1)}$ in terms of $I_0(\eta)$ [15] given by (A3) to (A5) in Appendix A may be inserted when numerically evaluating Ratio in (7.6) and (7.10).

Making use of

$$\frac{d}{d\eta} I_0(\eta) = \frac{-2}{1+4\eta} \left(I_0(\eta) - \frac{1}{2\eta} \right) \quad (7.11)$$

together with (7.9), Ratio in (7.10) becomes a function that depends on η and $I_0(\eta)$. The different dependence of $I_0(\eta)$ on η at large $\eta \gg 1$, where

$$I_0(\eta) \cong \frac{1}{2\eta} \left(1 - \frac{1}{6\eta} \right) + 0 \left(\frac{1}{\eta^3} \right), \quad (7.12)$$

and at small η of $\mu \leq \eta \ll 1$, where

$$I_0(\eta) \cong \ln \frac{1}{\eta} \left(1 - 2\eta \left(1 - \frac{1}{\ln \frac{1}{\eta}} \right) \right) + \dots, \quad (7.13)$$

determines the different behavior of the numerical results for Ratio to be presented next.

For the numerical evaluation of Ratio from (7.6) with (7.7) and (7.8) inserted, and of Ratio explicitly given in (7.10), we use the parameters¹⁰

$$\rho = \frac{4}{3}, \quad C_2 = 0.29, \quad C_1 = 0.31 \text{ GeV}^2, \quad m_0^2 = 0.15\text{GeV}^2. \quad (7.14)$$

We also note $\xi_L = 0.4$ (see (2.4)) and $\xi_2 = 0.5$ (see (6.14)).

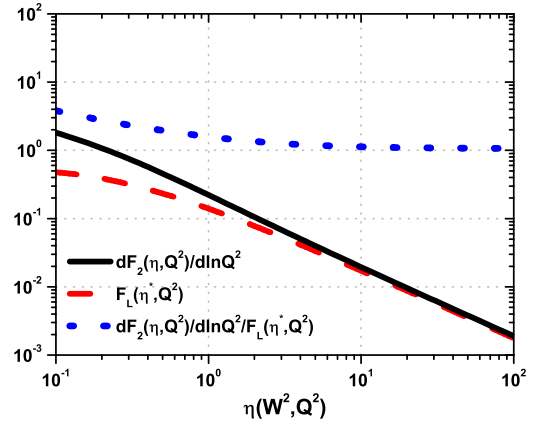


FIG. 10. The derivative of the structure function $F_2(\eta(W^2 = Q^2/x), Q^2)$ and the longitudinal structure function $F_L(\eta(W^2 = Q^2/x), Q^2)$ together with the ratio of both of them. The results are based on evaluating (7.7) and (7.8).

In Fig. 10, we show the derivative of the structure function as well as the longitudinal structure function according to (7.7) and (7.8), and their ratio defined by (7.6). For W^2 , the value of $W^2 = 10^5 \text{ GeV}^2$ was used.

⁹ In (7.10), the shift $\xi_2/\xi_L W^2$ in $\sigma_{\gamma p}\left(\frac{\xi_2}{\xi_L}W^2\right)/\ln\frac{\rho}{\mu\left(\frac{\xi_2}{\xi_L}W^2\right)}$ from (7.8) is ignored.

¹⁰ We add the comment that only the value of $C_1 = 0.31\text{GeV}^2$ is an entirely free fit parameter, whereas $\rho = \frac{4}{3}$ is a consequence of the enhanced transverse size of $q\bar{q}$ states originating from transversely relative to longitudinally polarized photons, and the exponent $C_2 = 0.29$ is accordingly fixed by (6.18). The value of $m_0^2 = 0.15\text{GeV}^2 < m_\rho^2$ is the starting point of the effective $q\bar{q}$ continuum, including the ρ^0, ω, ϕ peaks.

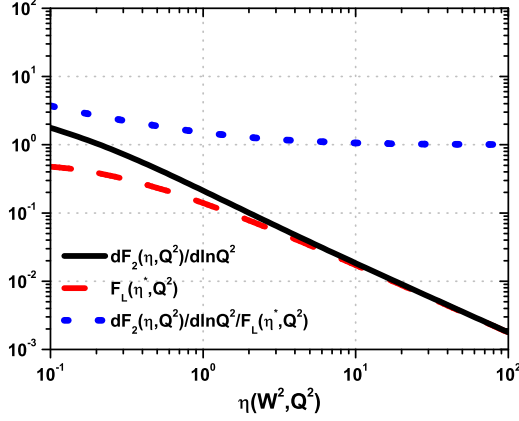


FIG. 11. As Fig. 10, however using the approximation $\sigma_{\gamma p}(W^2) \cong \text{const}$, compare to (7.10).

Since $\sigma_{\gamma p}(W^2)$ depends weakly on W^2 , we expect the numerical results of Fig. 10 not being drastically affected, if in (7.7) the term proportional to the derivative of $\sigma_{\gamma p}(W^2)$ is put to zero. The corresponding value of Ratio is explicitly given by (7.10). Comparison of the results in Fig. 11 with the ones in Fig. 10 indeed confirms that Ratio can reliably be evaluated according to the simple expression (7.10) upon insertion of $I_T^{(1)}$ and $I_L^{(1)}$ from (A.3) to (A.5).

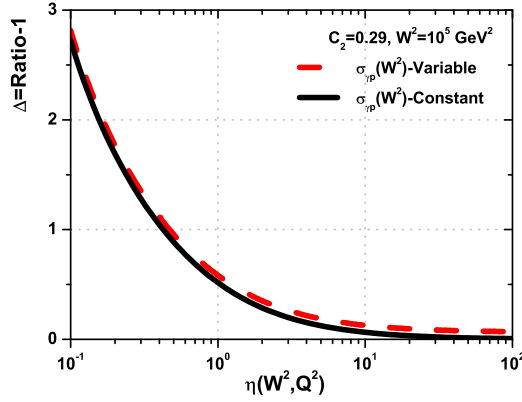


FIG. 12. The deviation from validity of the evolution equation obtained according to Figs. 10 and 11, respectively.

In Fig. 12, we show the deviation $\Delta\left(\eta\left(W^2 = \frac{Q^2}{x}\right), \mu(W^2)\right)$ of Ratio in (7.6) from unity on a linear scale. Remember, a value of unity means strict validity of the first DGLAP evolution equation (6.10) in the approximation (6.14) and (6.15). A deviation smaller than $\Delta\left(\eta\left(W^2 = \frac{Q^2}{x}\right), \mu(W^2)\right) \cong 0.1$

to 0.2 according to Fig. 12 requires $\eta(W^2, Q^2) \gtrsim 5$. The weaker increase of $F_L(\eta(x, Q^2), Q^2)$ relative to $F_2(\eta(x, Q^2), Q^2)$ with decreasing $\eta(x, Q^2)$ implies the substantial violation of the evolution equation reaching $\Delta(\eta(W^2, Q^2), \mu(W^2)) \cong 2.7$ at $\eta(W^2, Q^2) \cong 0.1$.

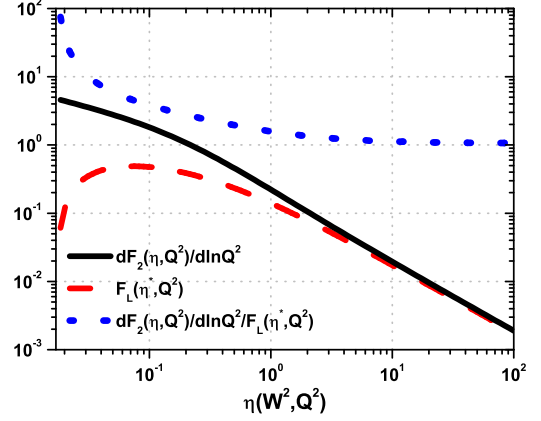


FIG. 13. The extension of Fig. 10 to the $Q^2 \rightarrow 0$ limit of $\eta(W^2, Q^2) \rightarrow \mu(W^2)$ for $W^2 = 10^5 \text{ GeV}^2$

Fig. 13 explicitly shows that the increase of Ratio relative to unity with decreasing η is strongly correlated to the necessary vanishing of the longitudinal structure function, $F_L(\eta(W^2, Q^2), \mu(W^2))$, in the denominator of Ratio in the limit of $\eta(W^2, Q^2) \rightarrow \mu(W^2)$ for $Q^2 \rightarrow 0$.

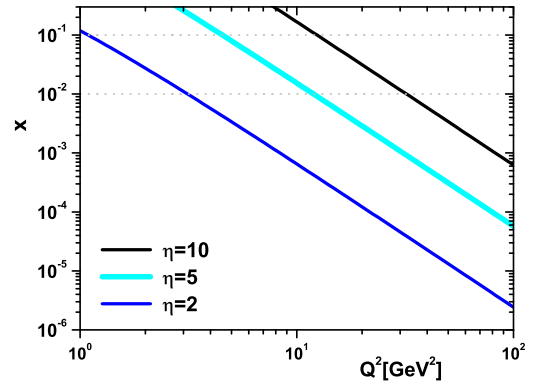


FIG. 14. The (Q^2, x) plane, showing the regions of $\eta(W^2, Q^2) > 5$ (approximate validity of conventional evolution) with $\Delta(\eta, \mu) \cong 0$, and of $\eta(W^2, Q^2) < 5$, where $\Delta(\eta, \mu) \neq 0$ occurs.

The value of $\eta \cong 5$ quantifies the region in the (Q^2, x) plane, see Fig. 14, below which the evolution equation becomes violated. It is amusing to note the coincidence of

this value with the value of $\eta \cong 5$, where the behavior of $\sigma_{\gamma^*p} \sim 1/\eta$ of the CDP in Fig. 1 turns from the region of color transparency to the region of hadronlike behavior. Above $\eta \cong 5$, we have pQCD-evolution or CDP-color-transparency, while below $\eta \cong 5$, we have a violation of conventional evolution that is equivalent to hadronlike saturation.

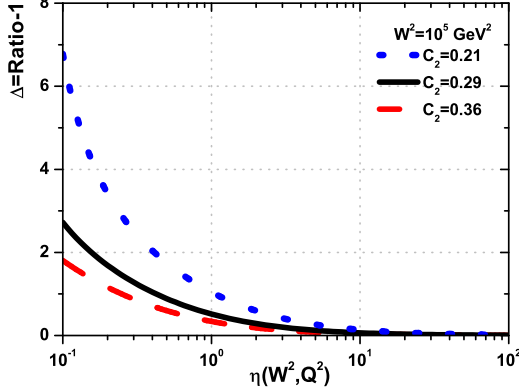


FIG. 15. The effect of the variation of ρ .

In Fig. 15, we address the question of the dependence of the above conclusion on the value of ρ that specifies the asymptotic behavior of the longitudinal-to-transverse ratio in photoabsorption via $R = 1/2\rho$. As long as precision experimental data on R , and accordingly on ρ , are lacking, it is interesting to vary ρ around its preferred value of $\rho = 4/3$, implying different values of the exponent C_2 according to (6.18). From Fig. 15, we infer that a change of ρ does qualitatively not significantly change our general conclusion obtained for $\Delta(\eta(W^2 = Q^2/x), Q^2)$.

We turn to the discussion of the gluon distribution function. Rewriting (7.6), and substituting the gluon distribution from (2.5), we find

$$\begin{aligned} \frac{\partial F_2(x, Q^2)}{\partial \ln Q^2} &= F_L\left(\frac{\xi_L}{\xi_2}x, Q^2\right) \\ &= \frac{\alpha_s(Q^2)}{9\pi} R_{e^+e^-} G\left(\frac{x}{\xi_2}, Q^2\right), \end{aligned} \quad (7.15)$$

where $R_{e^+e^-} = 10/3$ for four flavors of quarks. The factor $(1 + \Delta)^{-1}$ in (7.15), for $\Delta \neq 0$ represents a violation, or alternatively, a correction, to the evolution equation for the gluon distribution with decreasing η for $\eta(W^2 = Q^2/x, Q^2) \lesssim 5$.

In Figs. 10 to 13, we showed Ratio from (7.6) as a function of $\eta(W^2, Q^2)$ at fixed value of W^2 , chosen as $W^2 = 10^5 \text{ GeV}^2$, and the related variation of Q^2 . In connection with the extraction of the gluon distribution from DIS experimental data, one frequently uses a fixed value of Q^2 , chosen as low as $Q^2 = 1.9 \text{ GeV}^2 \cong 2 \text{ GeV}^2$,

as starting scale for the evolution of the gluon distribution with increasing Q^2 at fixed x .

TABLE III. Here $\Delta = \text{Ratio} - 1$ and $C_2 = 0.29$.

$Q^2[\text{GeV}^2]$	x	$W^2[\text{GeV}^2]$	η	$\Delta + 1$	$\frac{1}{\Delta + 1}$
2	10^{-2}	200	1.492	1.544	0.648
2	10^{-3}	2000	0.765	1.894	0.528
2	10^{-4}	20000	0.392	2.252	0.444
2	10^{-5}	200000	0.201	2.662	0.376
20	10^{-2}	2000	7.172	1.041	0.961
20	10^{-3}	20000	3.678	1.204	0.831
20	10^{-4}	200000	1.886	1.362	0.734
20	10^{-5}	2000000	0.967	1.563	0.640

In Table III, we show the results for $(1 + \Delta)^{-1}$ according to (7.6) with (7.7) and (7.8) for fixed $Q^2 = 2 \text{ GeV}^2$ and the typical range of $10^{-2} \leq x \leq 10^{-5}$, corresponding to an interval of η approximately given by $1.5 \geq \eta \geq 0.2$. According to Table III, we observe a dramatic correction factor to standard evolution of magnitude $0.6 \geq (1 + \Delta)^{-1} \geq 0.4$. This correction to evolution is due to a strong violation of the impulse approximation of pQCD at low Q^2 . The associated transition to hadronlike $(q\bar{q})p$ interactions is outside the range of validity of the standard evolution equations. It comes without surprise that global DIS data fits based on imposing evolution from a low- Q^2 -starting input scale “do not describe the deep inelastic scattering data in the low- x , low- Q^2 region very well” [6].

In Table III, in addition to the choice of $Q^2 = 2 \text{ GeV}^2$, we also give the results for the correction factor $(1 + \Delta)^{-1}$ at $Q^2 = 20 \text{ GeV}^2$. For $x = 10^{-2}$, with $(1 + \Delta)^{-1} = 0.96 \cong 1$, we have consistency with perturbative evolution, as expected. For sufficiently large W^2 , or $10^{-3} > x > 10^{-5}$, we observe the expected transition from unmodified pQCD evolution to hadronlike saturation.

In concluding this Section, we re-emphasize that the CDP provides a representation of the DIS experimental data that includes the transition to low Q^2 , including the limit of $Q^2 = 0$ photoproduction. We are convinced that the above results on the correction to pQCD evolution in the low x , low Q^2 region do not depend on the explicit form (Appendix A) of the underlying cross section formulae. Any representation including a smooth transition to $Q^2 = 0$ photoproduction must lead to qualitatively identical conclusions.

VIII. CONCLUSION.

We determined the low- x leading order gluon distribution of the proton from a representation of the DIS experimental data in the CDP. The CDP is unique by

providing a representation of the DIS experimental data in the low- x , low- Q^2 limit, including $Q^2 = 0$ photoproduction.

The CDP representation of the experimental data at large Q^2 ($20\text{GeV}^2 \lesssim Q^2 \lesssim 100\text{GeV}^2$ for data in the presently available energy range) is found to fulfill the constraints on the connection between the logarithmic derivative of $F_2(x, Q^2)$ and the gluon distribution function $G(x, Q^2)$ imposed by the evolution equation for $F_2(x, Q^2)$. The CDP of DIS at large Q^2 is equivalent to leading order pQCD.

Drastic modifications of evolution, uniquely determined by the CDP representation, are found at low Q^2 .

The origin of the breakdown of evolution is due to the mismatch between the logarithmic derivative of the structure function $F_2(x, Q^2)$ and the necessary decrease of $F_L(x, Q^2)$ in the low- Q^2 limit.

Our results strongly question the validity of the standard procedure in global fits to DIS data that start from a low- Q^2 input scale of e.g. $Q^2 = 1.9 \text{ GeV}^2$.

APPENDIX A

The explicit expressions for the functions $I_{L,T}^{(1)}(\eta(W^2, Q^2), \mu(W^2))$ in (3.2) are given by:

$$I_{L,T}(\eta(W^2, Q^2), \mu(W^2)) = I_{L,T}^{(1)}(\eta(W^2, Q^2), \mu(W^2)) \times (1 + 0(\mu(W^2))), \quad (\text{A.1})$$

where $I_L^{(1)}(\eta(W^2, Q^2), \mu(W^2))$ and $I_T^{(1)}(\eta(W^2, Q^2), \mu(W^2))$ are given by

$$\begin{aligned} I_L^{(1)}(\eta, \mu) &= \frac{\eta - \mu}{\eta} \\ &\times \left(1 - \frac{\eta}{\sqrt{1 + 4(\eta - \mu)}} \right. \\ &\times \ln \frac{\eta(1 + \sqrt{1 + 4(\eta - \mu)})}{4\mu - 1 - 3\eta + \sqrt{(1 + 4(\eta - \mu))((1 + \eta)^2 - 4\mu)}} \Bigg), \\ I_T^{(1)}(\eta, \mu) &= \frac{1}{2} \ln \frac{\eta - 1 + \sqrt{(1 + \eta)^2 - 4\mu}}{2\eta} \\ &- \frac{\eta - \mu}{\eta} + \frac{1 + 2(\eta - \mu)}{2\sqrt{1 + 4(\eta - \mu)}} \\ &\times \ln \frac{\eta(1 + \sqrt{1 + 4(\eta - \mu)})}{4\mu - 1 - 3\eta + \sqrt{(1 + 4(\eta - \mu))((1 + \eta)^2 - 4\mu)}}. \end{aligned} \quad (\text{A.2})$$

For $\mu(W^2) \ll 1$ (and $\eta(W^2, Q^2) \geq \mu(W^2)$) the functions $I_L^{(1)}(\eta, \mu)$ and $I_T^{(1)}(\eta, \mu)$ can be simplified to become

$$I_L^{(1)}(\eta, \mu) = \frac{\eta - \mu}{\eta} (1 - 2\eta I_0(\eta)) \quad (\text{A.3})$$

and

$$I_T^{(1)}(\eta, \mu) = I_0(\eta) - \frac{\eta - \mu}{\eta} (1 - 2\eta I_0(\eta)), \quad (\text{A.4})$$

where

$$I_0(\eta) = \frac{1}{\sqrt{1 + 4\eta}} \ln \frac{\sqrt{1 + 4\eta} + 1}{\sqrt{1 + 4\eta} - 1}. \quad (\text{A.5})$$

We also note that for the relevant range of $\eta \gg \mu$, or $Q^2 \gg \mu_0^2$, we may put $\mu = 0$ in (A.3) and (A.4).

APPENDIX B

In this Appendix we show the coefficients of the structure functions $F_2(x, Q^2)$ given in (4.1) as taken from ref. [22]. The coefficients in (4.1),

$$\begin{aligned} A(Q^2) &= a_0 + a_1 \ln \left(1 + \frac{Q^2}{\mu^2} \right) + a_2 \ln^2 \left(1 + \frac{Q^2}{\mu^2} \right), \\ B(Q^2) &= b_0 + b_1 \ln \left(1 + \frac{Q^2}{\mu^2} \right) + b_2 \ln^2 \left(1 + \frac{Q^2}{\mu^2} \right), \\ C(Q^2) &= c_0 + c_1 \ln \left(1 + \frac{Q^2}{\mu^2} \right), \\ D(Q^2) &= \frac{Q^2(Q^2 + \lambda M^2)}{(Q^2 + M^2)^2}, \end{aligned}$$

depend on the fit parameters listed in Table II.

TABLE B.1. The effective parameters at low x for $0.15\text{GeV}^2 < Q^2 < 3000\text{GeV}^2$ provided by the following values. The fixed parameters are defined by the Block-Halzen fit to the real photon-proton cross sections as $M^2 = 0.753 \pm 0.068 \text{ GeV}^2$, $\mu^2 = 2.82 \pm 0.290 \text{ GeV}^2$ and $c_0 = 0.255 \pm 0.016$.

parameters	value
a_0	$8.205 \times 10^{-4} \pm 4.62 \times 10^{-4}$
a_1	$-5.148 \times 10^{-2} \pm 8.19 \times 10^{-3}$
a_2	$-4.725 \times 10^{-3} \pm 1.01 \times 10^{-3}$
b_0	$2.217 \times 10^{-3} \pm 1.42 \times 10^{-4}$
b_1	$1.244 \times 10^{-2} \pm 8.56 \times 10^{-4}$
b_2	$5.958 \times 10^{-4} \pm 2.32 \times 10^{-4}$
c_1	$1.475 \times 10^{-1} \pm 3.025 \times 10^{-2}$
n	11.49 ± 0.99
λ	2.430 ± 0.153
χ^2 (goodness of fit)	0.95

-
- [1] L.A. Harland-Lang, A.D. Martin, P. Motylinski and R.S. Thorne, *Eur. Phys. J. C* **75**, 204 (2015).
- [2] S. Dulat et al., *Phys. Rev. D* **93**, no. 3, 033006 (2016).
- [3] R.D. Ball et al. [NNPDF Collaboration], *Eur. Phys. J. C* **77**, 663 (2017)
- [4] A. Buckley, J. Ferrando, S. Lloyd, K. Nordstrom, B. Page, M. Ruefenacht, M. Schoenherr and G. Watt, *Eur. Phys. J. C* **75**, 132 (2015).
- [5] H. Abramowicz et al. [H1 and ZEUS Collaborations], *Eur. Phys. J. C* **75**, 580 (2015).
- [6] M.R. Pelicer et al., *Eur. Phys. J. C* **79**, 9 (2019).
- [7] L.A. Harland-Lang, A.D. Martin, P. Motylinski and R.S. Thorne, *Eur. Phys. J. C* **76**, 186 (2016)
- [8] I. Abt, A.M. Cooper-Sarkar, B. Foster, V. Myronenko, K. Wichmann, M. Wing, *Phys. Rev. D* **94**, 034032 (2016).
- [9] L.N. Lipatov, *Sov. J. Nucl. Phys.* **20**, 94 (1975);
V.N. Gribov, L.N. Lipatov, *Sov. J. Nucl. Phys.* **15**, 438 (1972);
G. Altarelli, G. Parisi, *Nucl. Phys. B* **126**, 298 (1977);
Yu.L. Dokshitzer, *Sov. Phys. JETP* **46**, 641 (1977).
- [10] L.V. Gribov, E.M. Levin and M.G. Ryskin, *Phys. Rept.* **100**, 1 (1983).
- [11] A.H. Mueller and J.-W. Qiu, *Nucl. Phys. B* **268**, 427 (1986).
- [12] G. Cvetič, D. Schildknecht, A. Shoshi, *Eur. Phys. J. C* **13**, 301 (2000)
- [13] D. Schildknecht, *Nucl. Phys. B (Proc. Suppl.)* **99**, 121 (2001);
D. Schildknecht, B. Surrow, M. Tentyukov, *Phys. Lett. B* **499**, 116 (2001);
G. Cvetič, D. Schildknecht, B. Surrow, M. Tentyukov, *Eur. Phys. J. C* **20** (2001).
- [14] M. Kuroda and D. Schildknecht, *Phys. Rev. D* **85**, 094001 (2011).
- [15] M. Kuroda and D. Schildknecht, *Int. J. of Mod. Phys. A* **31**, 1650157 (2016).
- [16] J.J. Sakurai and D. Schildknecht, *Phys. Lett.* **40B**, 121 (1972);
B. Górczyca and D. Schildknecht, *Phys. Lett.* **47B**, 71 (1973);
H. Fraas, B.J. Read and D. Schildknecht, *Nucl. Phys. B* **86**, 346 (1975);
R. Devenish and D. Schildknecht, *Phys. Rev. D* **14**, 93 (1976).
- [17] D. Schildknecht, *Acta Physica Polonica* **B37**, 595 (2006).
- [18] M.Kuroda and D.Schildknecht, *Phys.Rev.D* **96**, 094013 (2017).
- [19] G. Altarelli, G. Martinelli, *Phys. Lett. B* **76**, 89;
A.D. Martin et al., *Phys. Rev. D* **37**, 1161 (1988);
A.M. Cooper-Sarkar et al., *Z. Phys. C* **39**, 281 (1988);
A.M. Cooper-Sarkar et al., *Acta Phys. Pol. B* **34**, 2911 (2003);
R.G. Roberts, *The Structure of the Proton*, (Cambridge University Press 1990).
- [20] D.Schildknecht, *Phys.Rev.D***104**, 014009 (2021).
- [21] Particle Data Group, *Phys. Rev. D* **86**, 1 (2012).
- [22] M.M. Block, L. Durand and P. Ha, *Phys. Rev. D* **89**, 094027 (2014).
- [23] M. Froissart, *Phys. Rev.* **123**, 1053 (1961).
- [24] M.M. Block, L. Durand and Douglas W. McKay, *Phys. Rev. D* **77**, 094003 (2008).
- [25] M.M. Block and L. Durand, *arXiv [hep-ph]: 0902.0372* (2009).
- [26] K. Prytz, *Phys. Lett. B* **311**, 286 (1993).